

1 Neural circuit basis of visuo-spatial working memory precision: a  
2 computational and behavioral study  
3  
4  
5  
6

7 Abbreviated title: Neural circuit basis of working memory precision  
8  
9

10 Rita Almeida<sup>1,2</sup>, João Barbosa<sup>1</sup>, Albert Compte<sup>1</sup>

11 <sup>1</sup>Institut d'Investigacions Biomèdiques August Pi i Sunyer (IDIBAPS), Barcelona, Spain

12 <sup>2</sup>Department of Neuroscience, Karolinska Institute, Stockholm, Sweden  
13  
14  
15  
16  
17

18 Corresponding author:

19 Albert Compte

20 Institut d'Investigacions Biomèdiques August Pi I Sunyer (IDIBAPS)

21 C/ Rosselló 149

22 08036 Barcelona

23 Spain

24 Fax: +34 93 3129408

25 Tel: +34 93 2275400 ext. 4151

26 E-mail: [acompte@clinic.ub.es](mailto:acompte@clinic.ub.es)  
27  
28  
29  
30

31 **Abstract**

32

33 The amount of information that can be retained in working-memory (WM) is limited. Limitations of  
34 WM capacity have been the subject of intense research, especially trying to specify algorithmic  
35 models for WM. Comparatively, neural circuit perspectives have barely been used to test WM  
36 limitations in behavioral experiments. Here, we used a neuronal microcircuit model for visuo-  
37 spatial WM (vsWM) to investigate memory of several items. The model assumes that there is a  
38 topographic organization of the circuit responsible for spatial memory retention. This assumption  
39 leads to specific predictions, which we tested in behavioral experiments. According to the model,  
40 nearby locations should be recalled with a bias, as if the two memory traces showed attraction or  
41 repulsion during the delay period depending on distance. Another prediction is that the previously  
42 reported loss of memory precision for increasing number of memory items (memory load) should  
43 vanish when the distances between items are controlled for. Both predictions were confirmed  
44 experimentally. Taken together, our findings provide support for a topographic neural-circuit  
45 organization of vsWM, they suggest that interference between similar memories underlies some  
46 WM limitations, and they put forward a circuit-based explanation that reconciles previous  
47 conflicting results on the dependence of WM precision with load.

48

49

50

51

52 **Keywords:** short-term memory, working-memory, precision, capacity, attractor model

53

54

55 Working-memory (WM) refers to the ability of actively retaining stimulus information over a short  
56 period of time and it is thought to be a core component of cognitive functions (Baddeley 1986,  
57 Conway et al. 2003). A hallmark of WM is that the information retained is limited. Currently, a  
58 significant effort is being devoted to characterizing the nature of WM capacity limitations, but their  
59 bases remain controversial (Luck and Vogel 2013, Ma et al. 2014). Important points of discordance  
60 have been whether or not the number of items in WM can be increased at a cost in precision (Bays  
61 and Husain 2008, Zhang and Luck 2008) and whether the similarity of the items to memorize  
62 improves (Johnson et al. 2009, Lin and Luck 2009) or degrades (Elmore et al. 2011) WM  
63 performance.

64 Recently, a neuronal circuit perspective is entering these debates: electrophysiological experiments  
65 have started to investigate the neural basis of multiple item WM (Buschman et al. 2011, Warden and  
66 Miller 2007, Lara and Wallis 2014), and neural-circuit modeling has been used to link cellular and  
67 network mechanisms with behavior to understand WM capacity limitations (Macoveanu et al. 2006,  
68 2007, Edin et al. 2009, Wei et al. 2012, Wimmer et al. 2014, Bays 2014, Papadimitriou et al. 2015).  
69 Most of these models are variations of a model (Compte et al. 2000) developed to be consistent with  
70 neurophysiological data from behaving monkeys (Funahashi et al. 1989). They rely on the  
71 assumption that there is a topographic structure in the circuits supporting vsWM, which implements  
72 a continuous attractor mechanism responsible for the retention of spatial memory. Some evidence  
73 from fMRI (Schluppeck et al. 2006, Kastner et al. 2007) and electrophysiology studies  
74 (Constantinidis et al. 2001, Inoue and Funahashi 2002) supports a coarse degree of spatial WM  
75 maps in parietal and prefrontal cortex. Recently, neural evidence for attractor dynamics on a fine  
76 vsWM spatial map in prefrontal cortex has also been found (Wimmer et al. 2014). However,  
77 additional implications of such a spatial memory map for the relation between vsWM precision,  
78 capacity and stimulus similarity remain untested. We aimed here to advance our understanding of  
79 the neuronal underpinnings of vsWM by explicitly testing the assumption of a topographic structure  
80 of the vsWM buffer. One implication of this structure is that the efficiency with which different

81 items are memorized should depend on their relative locations, since stronger interference of  
82 memory traces would be expected for nearby items. Using simulations we predicted an attractive  
83 bias when remembering locations of two nearby items, for very short inter-item distances. This  
84 prediction was validated in behavioral experiments in humans. We then sought to address how these  
85 interferences affected the relationship between memory load and precision. In our model, the effect  
86 of load on memory precision was largely accounted for by changes in inter-item distance with load.  
87 Behavioral data confirmed this prediction. We finally tested in an additional experiment that  
88 behavioral data was better explained by memory attraction than by memory swapping (Bays et al.  
89 2009), and we also confirmed that intermediate distances between memorized items were  
90 characterized by a repulsive memory bias. The importance of our work is three-folded. First, we  
91 provide new experimental evidence concerning interference in vsWM. Second, we test a critical  
92 assumption of an important class of models of vsWM. Third, we put forward a plausible  
93 explanation reconciling previous results concerning the dependence of memory precision on load  
94 and concerning similarity effects on performance.

95

96

## 97 **Materials and Methods**

### 98 **Model**

99 We used a previously proposed computational model (Compte et al. 2000, Edin et al. 2009) to study  
100 the precision of vsWM of multiple items. The model (Compte et al. 2000) was originally developed  
101 to account for a candidate neuronal mechanism for vsWM, namely the selective sustained elevated  
102 neuronal firing of the prefrontal cortical neurons of monkeys performing a vsWM task (Funahashi  
103 et al. 1989). The model consists of a network of interconnected excitatory and inhibitory spiking  
104 neurons. The neurons encode the spatial location of fixed-eccentricity visual stimuli in angle  $\theta$ . That  
105 is, they encode positions (in angle) on a circle. Presentation of a stimulus at location  $\theta$  is simulated  
106 by increasing the external input to the corresponding excitatory neurons. The selective response of

107 the neurons in the network is maintained due to the structured connectivity of the network.  
 108 Excitatory neurons encoding for nearby angles have stronger than average connections, which is  
 109 essential for a selective group of neurons to sustain elevated spiking after stimulus cessation  
 110 (Compte et al. 2000)

111 The parameter values used were as in the IPS circuit described in Edin et al. 2009, for a network  
 112 capacity of 2 items. The model had 1024 excitatory and 256 inhibitory leaky integrate-and-fire  
 113 neurons (Tuckwell 1988). The neuronal selectivity was imposed by external inputs, assumed to  
 114 originate in upstream areas of the dorsal pathway. Specifically, the presence of a visual stimulus at  
 115 an angle  $\theta_{stim}$  was modeled by increasing the external input to excitatory neurons with preferred  
 116 direction around  $\theta_{stim}$ . The strength of the external input to a neuron encoding  $\theta$  decayed with the  
 117 distance to  $\theta_{stim}$  according to  $I_{stim}(\theta, \theta_{stim}) = \alpha \exp(\mu [\cos(2\pi / 360(\theta - \theta_{stim})) - 1])$ , where  
 118  $\alpha = 0.025$  nA and  $\mu = 39$ .

119 The integrate-and-fire neuron model describes how the membrane voltage  $V_m$  integrates incoming  
 120 inputs until a certain threshold value  $V_{th}$  is reached and an action potential or spike is fired. After  
 121 reaching the threshold,  $V_m$  is reset to  $V_{res}$  for a refractory time period  $\tau_{ref}$  before continuing to  
 122 integrate inputs. The equation describing the sub-threshold changes in  $V_m$  is:

$$C_m \frac{dV_m}{dt} = -g_L(V_m - E_L) - I_{syn} - I_{ext}$$

123  
 124 Each cell is then characterized by the total membrane capacitance  $C_m$ , the total leak conductance  
 125  $g_L$ , the leak reversal potential  $E_L$  and by  $V_{th}$ ,  $V_{res}$ , and  $\tau_{ref}$ . For excitatory neurons the values  
 126 used were:  $C_m = 0.5$  nF,  $g_L = 25$  nS,  $E_L = -70$  mV,  $V_{th} = -50$  mV,  $V_{res} = -60$  mV,  $\tau_{ref} = 2$  ms; and  
 127 for inhibitory neurons:  $C_m = 0.2$  nF,  $g_L = 20$  nS,  $E_L = -70$  mV,  $V_{th} = -50$  mV,  $V_{res} = -60$  mV,  
 128  $\tau_{ref} = 1$  ms.

129 The network of neurons was organized according to a ring structure: excitatory and inhibitory

130 neurons were spatially distributed on a ring so that nearby neurons encoded nearby spatial locations.  
 131 An illustration of this structure is shown in Figure 1A. Connections between neurons were spatially  
 132 tuned so that nearby neurons with similar preferred directions had stronger than average  
 133 connections, while distant neurons had weaker connections. The distance dependent connection  
 134 strength  $g_{syn,ij}$  between cells  $i$  and  $j$  was described by  $g_{syn,ij} = W(\theta_i - \theta_j)G_{syn}$ , where

$$W(\theta_i - \theta_j) = J^- + (J^+ - J^-)e^{-(\theta_i - \theta_j)^2/2\sigma^2}$$

135

136 and  $J^-$  was set to satisfy a normalization condition (see Compte et al. 2000). The parameters used  
 137 were:  $\sigma_{E \rightarrow E} = 9.4$  deg,  $\sigma_{E \rightarrow I} = \sigma_{I \rightarrow E} = 32.4$  deg,  $J_{E \rightarrow E}^+ = 5.7$ ,  $J_{E \rightarrow I}^+ = J_{I \rightarrow E}^+ = 1.4$ ,  $J_{I \rightarrow I}^+ = 1.5$ . Thus,  
 138 the connectivity between excitatory and inhibitory neurons was wider and flatter than that between  
 139 excitatory neurons. The connectivity between inhibitory neurons was not spatially tuned. The  
 140 strengths of the connections were  $G_{E \rightarrow E} = 0.7$  nS,  $G_{E \rightarrow I} = 0.49$  nS,  $G_{I \rightarrow E} = 0.935$  nS,  
 141  $G_{I \rightarrow I} = 0.7413$  nS. Apart from stimulus selective inputs, all neurons received uncorrelated random  
 142 background excitatory input. The times of incoming action potentials were modeled according to a  
 143 Poisson process with rate 1,800 sp/s. The conductances of this input were  $g_{ext \rightarrow E} = 6.5$  nS,  
 144  $g_{ext \rightarrow I} = 5.8$  nS. The effect of incoming action potentials was modeled through conductance-based  
 145 synapses. Thus, postsynaptic currents followed the equation:

$$I_{syn} = g_{syn} s (V_m - V_{syn}),$$

146

147 where  $g_{syn}$  is the synaptic conductance,  $s$  is the synaptic gating variable, and  $V_{syn}$  is the synaptic  
 148 reversal potential ( $V_{syn} = 0$  for excitatory synapses,  $V_{syn} = -70$  mV for inhibitory synapses).  
 149 Recurrent excitatory connections were modeled to follow the dynamics of NMDAR mediated  
 150 transmission, external excitatory inputs to follow AMPAR mediated transmission and inhibitory  
 151 inputs to follow GABA<sub>A</sub>R transmission. The dynamics of the AMPAR and GABA<sub>A</sub>R synaptic

152 gating variables were modeled as an instantaneous jump of magnitude 1 when a presynaptic action  
 153 potential occurred, followed by an exponential decay with time constant 2 ms for AMPA and 10 ms  
 154 for GABA<sub>A</sub>. The NMDAR conductance was voltage-dependent and this was modeled by  
 155 multiplying  $g_{syn}$  by  $1 / (1 + [Mg^{2+}] \exp(-0.062 V_m) / 3.57)$ , with  $[Mg^{2+}] = 1.0$  mM. The dynamics of the  
 156 NMDAR synaptic gating were modeled by:

$$157 \quad \frac{ds}{dt} = \frac{-s}{\tau_s} + \alpha_s x (1-s), \quad \frac{dx}{dt} = \frac{-x}{\tau_x} + \sum \delta(t-t_i)$$

158 where  $s$  is the gating variable,  $x$  is a synaptic variable proportional to the neurotransmitter  
 159 concentration in the synapse,  $t_i$  are the presynaptic action potential times,  $\tau_s = 100$  ms is the decay  
 160 time,  $\tau_x = 2$  ms controls the rise time, and  $\alpha_s = 0.45$  kHz controls the saturation properties of  
 161 NMDAR channels.

162 Predictions from the model were derived from simulation results. Each simulation started with 100  
 163 ms of baseline activity, followed by stimulus specific stimulation during 500 ms and ended with a  
 164 500 ms delay period (Figure 1B,D). The locations of the memories for each item were read out  
 165 using Bayesian or maximum *a posteriori* decoding assuming an extended Poisson model as  
 166 described by Zemel et al. (1998). This encoding-decoding framework was developed to handle  
 167 situations where more than a single value (for example several locations) should be encoded and  
 168 decoded from the neural activity of a population of neurons. Using this method, from the neuronal  
 169 activity one determines a whole probability distribution over possible locations instead of a single  
 170 most likely location. This allows for the encoding and decoding of different locations. The  
 171 decoding distribution of items, that is the probability distribution of angular locations  $\phi_j$ , was  
 172 estimated given the activity of the excitatory neurons in the last 100 ms of the delay period. For this,  
 173 we used the function *sqp* from the software package GNU Octave (Eaton et al., 2009) to maximize  
 174 an approximation of the logarithm of the probability distribution of angular locations  $\phi_j$  (equation  
 175 17 of Zemel et al. 1998):

176

$$AP(\phi_j) = \sum_i r_i \log \left[ \sum_j \phi_j f(x_{ij}) \right] - \varepsilon (\phi_j - \phi_{j+1})^2$$

177

178 where  $r_i$  is the activity of neuron  $i$ ,  $x_{ij}$  is the difference between the preferred angles of neurons  $i$   
179 and  $j$ ,  $f(x_{ij})$  is a neuronal tuning function assumed to be Gaussian with standard deviation 10 deg,  
180 set to match the dispersion of the network response to one item (the tuning), and  $\varepsilon = 10^{-7}$  is a  
181 weighting coefficient of the smoothness prior  $\sum (\phi_j - \phi_{j+1})^2$ , which imposes smoothness across  
182 angular locations  $\phi_j$ . Single values for the estimated locations of memorized items were found by  
183 determining the locations  $\phi_j$  corresponding to the local maxima of  $AP(\phi_j)$ . Before estimation, the  
184 spiking activity was resampled to a resolution of 360 for efficiency. Memory imprecision for each  
185 stimulus item was quantified as the distance in angle between that item location and the closest  
186 local maximum of the posterior probability of item locations, with the restriction that the distance  
187 had to be smaller than 35 deg. This restriction assured that in cases where the memory trace  
188 vanished during the delay period the particular item was not attributed to a memory trace and  
189 instead it was counted as forgotten. In these cases the read-out was taken to be a random location on  
190 the circle to mimic a subject guessing a forgotten spatial location. In cases where memory traces  
191 merged, the items were attributed to the same local maximum of the posterior probability. To study  
192 the effect of the distance between two simultaneously presented items on WM performance, we ran  
193 100 simulations for different angular distance  $\Delta\theta$  between the two items (Figure 2A,  $\Delta\theta$  from 45  
194 to 90 deg). From these simulations we calculated the angular distance between remembered  
195 locations and corresponding item locations. This angular distance is a measure of error or bias in  
196 remembered location. If this bias was in the direction of the location of other memorized items  
197 (Figure 1B) we defined it as a positive memory bias, corresponding to the attraction of memory  
198 traces. If the bias was in the direction opposed to close-by memorized items we defined it as a  
199 negative memory bias, corresponding to the repulsion of memory traces. To study the relation  
200 between precision and load for different positions of the items we ran 300 simulations for each load  
201 and for each stimulus distribution (far or random cases, Figure 2B). For trials labeled random, items



202 were simulated at random around a circle, with the restriction that they could not be closer than 33  
203 deg. In trials labeled far, we applied the additional condition that at least one item per simulation  
204 (*far item*) was more than 80 deg apart from all other items. The results were then calculated probing  
205 these far items. In particular, we computed standard deviations of the angular distances between  
206 remembered locations and corresponding item locations. We also calculated psychometric curves  
207 for each load and stimulus distribution. To this end, we counted for all simulations and for a given  
208 probed angular distance how many memory traces were counter-clockwise in relation to the probed  
209 distance. The results are presented as proportion of memories counter-clockwise to the probed  
210 location, as a function of angular distance between the probe and item. We fitted these proportions  
211 using probit models with angular distance as independent variable. The probit models were  
212 estimated using the Statistics Toolbox of Matlab.

213 The integration of the model equations was done using a second order Runge-Kutta algorithm. The  
214 simulations were performed with code implemented in C++.

215  
216

## 217 **Behavioral experiments**

218 We used a vsWM task where the subjects were presented with a set of dots and had to judge after a  
219 blank delay period whether a re-appearing dot had been displaced clockwise or counter-clockwise.  
220 The experimental paradigm is schematically illustrated in Figure 3A. The stimuli were displayed on  
221 a computer screen, on gray background. Participants sat ~60 cm from the screen and were asked to  
222 fixate the central black square present during the whole trial time. Participants were also asked to  
223 memorize each item *per se* and avoid remembering the dots as a pattern. To limit the efficacy of  
224 pattern encoding strategies, we introduced specific constraints for the location of the items in each  
225 trial so that geometric symmetries or cardinal directions were avoided (see below).

226 Each trial started with the presentation of a central fixation cue for 1 s, followed by the presentation  
227 of the visual stimulus for 1 s. The stimulus consisted of a set of three or four colored dots (*items*)  
228 presented on an invisible circle centered on the fixation point and with a radius subtending a visual

229 angle of 12.4 deg. The items were never presented on the horizontal and vertical diameters of the  
230 circle. The colors were attributed randomly to the different items for each trial. The stimulus was  
231 followed by 100 ms presentation of a mask consisting of an annulus (radii in visual angle 11.5 deg  
232 and 13.2 deg) of a pixelized noise pattern in a gray scale. The mask was followed by the  
233 presentation of a probe (in no-delay trials) or by a delay of 1 or 3 s (delay trials) followed by  
234 presentation of a probe. The probe stimulus consisted of one of the stimulus dots displaced  
235 clockwise or counterclockwise on the invisible circle relative to the original stimulus location. The  
236 task consisted in judging the direction of displacement and reporting it by pressing one of two  
237 possible keys in a keyboard. Participants were given 5 s to respond and always did it before this  
238 time had elapsed. The probe was displayed until the subjects responded. Participants were trained  
239 until they showed no problems in associating the directions with the respective keys. It always took  
240 less than 48 trials to automatize the association. The amount of displacement in visual angle of the  
241 probe item was 0.9, 1.3 or 1.7 deg (4, 6, and 8 deg along the circle), and the probe could not be in a  
242 different hemifield than the corresponding target item. In half of the trials the memory of an item  
243 that was far from all other items was probed. For these trials, half showed all items far from each  
244 other (minimal distance between items was 70 deg along the circle for load 3 and 50 deg for load 4).  
245 These trials are referred to as far trials in Figure 3 and as balanced trials in Figure 4. The other half  
246 of trials where an item far from all other was probed had two non-probed items close to each other  
247 (minimal distance along the circle from the probed item to another item was 90 deg for load 3, and  
248 50 deg for load 4). These trials are referred to as unbalanced trials in Figure 4. Different restrictions  
249 on distances were imposed on trials with load 3 and 4 to ensure that a substantial part of the circle  
250 was spanned by the locations (in angle) of the items. With this we wanted to minimize possible  
251 effects of attention that could appear if subjects could focus on a small portion of the circle, and  
252 strategies to store items as geometric patterns. These restrictions resulted in trial types with  
253 balanced (invariant) and unbalanced (varying) distances across loads, which we used to demonstrate  
254 the *Prediction of conditional dependence of precision on load* (see *Results*). In half of the total

255 number of trials the memory of an item located close to another item was probed (the distance  
256 between nearby items was between 10 and 20 deg along the circle, corresponding to a visual angle  
257 between 2.2 and 4.2 deg). In half of these trials the probe was displaced outwards or away from the  
258 nearby item and in the other half of trials the probe was displaced inwards or towards the nearby  
259 item. For each trial type, trials were balanced in relation to relative positions of the dots in the  
260 stimulus, the displacements of the probe, the number of items and the presence or absence of a  
261 delay period. The experiment was run in sessions of 48 trials, lasting around 5 minutes. Within each  
262 session the delay was fixed, and each participant ran 4 sessions for each of 3 possible delays (no-  
263 delay, 1 s or 3 s). Type of trial, direction and amount of displacement, color of dots and hemifield of  
264 the probed dot were randomized and balanced within each session. The order of the sessions was  
265 randomized across participants. 8 healthy participants (4 females) took part in the experiment, with  
266 ages between 23 and 37 years and normal or corrected-to-normal vision.

267 To check for evidence of errors due to misremembering the colors of the items (Bayes et al. 2009,  
268 Pertzov et al. 2012, Ma et al. 2014), we conducted a variant of this vsWM experiment. The  
269 experimental paradigm is schematically illustrated in Figure 5A. The experiment was exactly as the  
270 one described above, except for the response period. After the delay period the fixation dot changed  
271 from black to the color of one of the previously presented items. The subject was required to  
272 respond by indicating the remembered position of the item matching the color of the fixation mark.  
273 To indicate the remembered position, the subjects used a pressure-sensitive tablet and pen. The  
274 movement of the pen was reproduced in the visual display as a cursor so that the subjects saw the  
275 colored fixation dot moving from the fixation spot to the remembered position. The subject  
276 indicated the reported position by releasing the pen from the tablet. All trials had a delay of 3s and  
277 separation between nearby items ranged from 3.1 to 4.4 deg of visual angle (14 to 20 deg on the  
278 circle). Data was acquired from 4-8 sessions from each of 9 healthy participating subjects (4  
279 females), ages between 21 and 27 years old and showing normal or corrected-to-normal vision.  
280 For each subject, sessions were typically acquired in different days. Some participants completed

281 fewer sessions, because they were not available for more data collection. The trials where the  
282 probed item was near another item were classified into two trial types, according to the probed item  
283 being clockwise or counter-clockwise relative to the nearby item.

284 Participants for both experiments were recruited among a local community of researchers and  
285 students from the Institut d'Investigacions Biomèdiques August Pi i Sunyer (IDIBAPS). The  
286 experiments were conducted with the approval of the CEIC at the Hospital Clínic in Barcelona  
287 (Spain) and informed consent was obtained from all participants before the experiments took place.

288

### 289 **Behavioral data analysis**

290 Behavior from the first experiment was measured as the number of correct trials. The results were  
291 analyzed using generalized mixed probit models in R (R Development Core Team, 2013), MASS  
292 package (Venables and Ripley 2002), with participant as a random factor. For the first test of our  
293 first prediction (see *Results*), trial type, delay and the interaction between trial type and delay were  
294 used as independent variables or predictors. For the second test of this prediction, the amount of  
295 probe displacement was also included.

296 Since the interaction term was significant in both cases, the data was separated according to  
297 delay and a model was fitted using trial type as predictor for test 1 and trial type, amount of probe  
298 displacement and the interaction between these two variables as predictors for test 2. For the test of  
299 the second prediction (see *Results*), trial type, delay, load and amount of probe displacement were  
300 used as independent variables. The model also included interactions between these variables. Since  
301 an interaction between delay, trial type and displacement was found to be significant the data was  
302 separated according to the delay. A new model without the delay variable was fitted. Since for the  
303 delay trials we found an interaction between displacement, load and trial type, the data was further  
304 divided according to trial type. For these new data partitions, a model was fitted using amount of  
305 probe displacement, load and the interaction between these two variables as predictors.

306 Behavior in the second experiment was analyzed in three ways. For testing the prediction of

307 attraction, the data was analyzed using a linear mixed model, with participant as a random factor  
308 and trial type as a predictor. To test the dependency of memory biases on inter-item distance (Figure  
309 6) we fitted cumulative Gaussians to the cumulative fraction of error reports (Figure 5B),  
310 collapsing clockwise and sign-inverted counterclockwise errors, and we used the fitted mean as an  
311 estimate of the memory bias (Figure 6A). Positive biases thus reflected attraction and negative  
312 biases reflected repulsion of the two memories. In Figure 6B we assessed the significance of each  
313 participant's memory bias with a two-sample *t*-test on the error distributions of clockwise and  
314 counterclockwise trials. We used a multinomial regression model to test if the relative incidence of  
315 significant repulsion biases as compared with attraction biases increased with inter-item distance in  
316 our subject population (Figure 6B). The dependent variable could take 3 possible values: attraction,  
317 repulsion or no effect. For each subject, we got 3 measurements of the dependent variable,  
318 corresponding to 3 bins of distances between items (Figure 6). The model included an intercept and  
319 the inter-item distance (taking values 3, 3.75, 4.2) as predictors. The link function was a generalized  
320 logit function.

321 Finally, in order to test alternative statistical models, the data was fitted to three statistical models  
322 detailed below using a custom expectation maximization algorithm for the maximum likelihood  
323 estimation (Dempster et al. 1977) based on publicly available code (Bays et al. 2009,  
324 <http://www.paulbays.com>). Model comparison was done using Akaike information criterion (AIC)  
325 (Akaike 1974), which is a measure of the relative quality of a statistical model for a given data set.  
326 Information loss of one model relative to another is then calculated by the differences between AIC  
327 values (Burnham and Anderson 2004). The information loss  $\Delta AIC$  of each model compared to the  
328 best (the one with the lowest AIC) was calculated for each subject and then averaged across  
329 subjects. The relative likelihood of model *i* relative to the best model was computed as  
330  $\exp(\Delta AIC_i/2)$ .

331

332

333 **Statistical models**

334 A possible explanation for the errors in the task could be a wrong association (or binding) of color  
335 and location of the items (Bays et al. 2009, Pertzov et al. 2012, Ma et al. 2014). To access whether  
336 interference (attraction) between memory traces of item locations or misbinding best explains our  
337 experimental results we used three statistical models, hereby called *swap*, attraction and  
338 *attraction+swap* models. All the models assume that the experimental distribution  $f_{EXP}(\Delta\theta)$  of  
339 errors in reported angle  $\Delta\theta$  can be described as a mixture of von Mises components (Figure 5C), a  
340 circular analogue of the Gaussian distribution with dispersion parameter  $\sigma$ , defined as

341 
$$\phi_{\sigma}(\Delta\theta) = \exp\left[\cos(\Delta\theta) / \sigma^2\right] / (2\pi I_0(1 / \sigma^2))$$
, with  $I_0$  the modified Bessel function of order 0.

342 *Swap model*. This model is the one introduced by Bays et al. (2009), to account for performance on  
343 a recall task where both stimuli and responses are chosen from a circular parameter space. The  
344 model assumes that the experimental distribution can be described as a mixture of 3 components:

$$f_{EXP}(\Delta\theta) = p_t \phi_{\sigma}(\Delta\theta) + p_{nt} \frac{1}{n} \sum_i \phi_{\sigma}(\Delta\theta_i^*) + p_u \frac{1}{2\pi}$$

345

346 The first component, weighted by  $p_t$ , describes the responses to correctly remembered items,  
347 where the subject reports the remembered position with some uncertainty around the error to the  
348 actual location of the target item. This is modeled using the von Mises distribution centered around  
349 the error to the target  $\Delta\theta$ , with dispersion parameter  $\sigma$ . The second component, weighted by  $p_{nt}$ ,  
350 describes the responses to nearby non-target items, i.e. responses indicating the remembered  
351 location of a non-target item (item with a color different from the probed color). Such responses  
352 reflect errors in the binding of color and location of an item (*swap errors*, Bays et al. 2009). This is  
353 also modeled using a von Mises distribution with dispersion parameter  $\sigma$ , but now centered on the  
354 error to the non-target location  $\Delta\theta^* = \theta - \theta_{nt}$ . Finally, the third component describes the situation  
355 where the item location is forgotten and the subject guesses according to a uniform distribution. The

356 model has 3 parameters  $p_t$ ,  $p_{nt}$  and  $\sigma$ , which can be estimated to fit the experimental data.

357 *Attraction model.* In this model the subjects' reports are described by a unimodal von Mises  
358 distribution centered on a location intermediate between the target and non-target items. This  
359 displacement would occur as a result of the attraction of coding bumps in our more detailed model  
360 of Figure 1. This model drops one of the components, the possibility of having swap errors, and  
361 introduces a bias  $b$  in the mean, representing the attraction effect:

$$f_{EXP}(\Delta\theta) = p_t \phi_\sigma(\Delta\theta + b) + p_u \frac{1}{2\pi}$$

362

363 Since nearby items were separated by different distances  $\delta_i$ , the bias  $b_i$  in individual trials was  
364 constrained to be a fraction of  $\delta_i$ :  $b_i = b' \delta_i$ , and we estimated the constant factor  $b'$ . In total, the  
365 model has 3 parameters  $p_t$ ,  $\sigma$  and  $b'$ , which can be estimated to fit the measured data.

366

367 *Attraction+swap model.* Finally, both errors might co-exist: in some trials the two features of the  
368 stimulus are misbound, but in any case reports (to target or to non-target items) are biased towards  
369 the nearby stimulus. This model is the same as the swap model but with one more parameter for the  
370 bias:

$$f_{EXP}(\Delta\theta) = p_t \phi_\sigma(\Delta\theta + b) + p_{nt} \frac{1}{n} \sum_i^n \phi_\sigma(\Delta\theta_i^* - b) + p_u \frac{1}{2\pi}$$

371

372 Note that the bias  $b$  (as above,  $b_i = b' \delta_i$ ) affects equally both the responses to target and non-target  
373 items. This model has 4 parameters  $p_t$ ,  $p_{nt}$ ,  $\sigma$ , and  $b'$  which can be estimated to fit the experimental  
374 data.

375

376

## 377 **Results**

378

### 379 **Predictions from the computational model**

380 We used an existing computational model (Compte et al. 2000, Edin et al. 2009) to study vsWM of  
381 several simultaneously presented items. For simplicity, we considered only the memory storage of  
382 locations at equal eccentricity, so that the item locations could be labeled by an angle  $\theta$ . The model  
383 consists of a one-dimensional network of neurons connected in a topographic manner (Figure 1A),  
384 so that neurons encoding nearby locations have stronger connections than neurons encoding far  
385 apart locations. This structure enables the network to sustain stimulus selective activity during a  
386 delay period (Compte et al. 2000). When plotting the activity of excitatory neurons organized  
387 according to their selectivity (Figure 1B, C), the sustained spiking corresponding to a memory trace  
388 is visualized as a spatially localized bump of activity in the network ( $y$ -axis) that is persistent over  
389 time ( $x$ -axis). The continuous topographical structure of the network connectivity implies that  
390 memory traces maintained simultaneously are not independent and interfere with each other. It  
391 further implies that the interference is dependent on the relative locations of the angles memorized,  
392 more interference being expected for nearby items than for far-apart items. Possible types of  
393 interference of memory traces are attraction (Figure 1B), repulsion and extinction (Figure 1C). To  
394 study the effects of interference on vsWM for several items we started by considering two items and  
395 we systematically changed the angle  $\Delta\theta$  separating them. We measured memory bias as the angular  
396 distance between cued locations and memory locations encoded in network activity 0.5 s after  
397 stimulus extinction (*Materials and Methods*). Further we defined memory bias as being positive  
398 when it reflected attraction between memory traces and negative when it reflected repulsion  
399 between memory traces. Figure 2A shows that there is a large attraction effect for angles smaller  
400 than 60, and an intermediate repulsion effect for intermediate angles, which disappears as  $\Delta\theta$   
401 increases. Our simple model cannot match quantitatively the conditions of a real cortical circuit and  
402 hence we do not know in what range of  $\Delta\theta$  we should expect the different behaviors, attraction and



403 repulsion. However, we do know that for small angles between items we should have an attraction  
404 effect while for very large angles we should have no effect. Based on this we sought to mainly test  
405 our model using items very close by or in relative isolation, where we would not need to search for  
406 subject-dependent angles leading to repulsion. Hence, the first prediction we aimed at testing in  
407 behavioral experiments was that vsWM for adjacent locations should show biases consistent with a  
408 perceived attraction between the two items. We refer to this prediction as the *Prediction of*  
409 *attraction biases*. We have however also checked *a posteriori* our experimental data for evidence of  
410 the predicted repulsive effects at intermediate inter-item distances (see “Testing repulsive biases”).

411  
412 We then studied how interference affected precision in our network model when the number of  
413 items to be memorized (the load) increased. We measured the standard deviation over trials of  
414 report errors  $\sigma$ , in simulation series where different number of items (from 1 to 4) were presented  
415 to the network for memorization. We considered two cases. In the first case, we minimized  
416 interference by keeping distances between items large (*far case*). In the second case, the items were  
417 located at random (*random case*). We found that  $\sigma$  depended markedly on load in the random case,  
418 while it remained relatively constant as load changed in the far case (Figure 2B). This was because  
419 when items were randomly placed, the probability of having items separated in the range of  
420 interference (Figure 2A) increased with load. When this probability was only allowed to change  
421 minimally with load, as in the far case,  $\sigma$  remained practically constant.

422 This effect can be demonstrated in the shape of psychometric curves. We used the same simulations  
423 as above to derive psychometric curves showing the proportion of items that are judged counter-  
424 clockwise to a probed location (Materials and Methods), as a function of angular distance between  
425 probed location and item location (Figure 2C, D). For the simulations where only far items were  
426 probed, the psychometric curves changed minimally with load (Figure 2C). For the simulations  
427 where items were randomly placed, the psychometric curves for loads 3 and 4 showed greater  
428 difference (Figure 2D). The different slopes of the psychometric curves reflect different memory  
429 precisions for loads 3 and 4, consistent with greater interference of neighboring bumps in load 4

430 trials. So, our second prediction was that the previously reported loss of precision with load (Bays  
431 and Husain 2008) would largely depend on the relative positioning of the items to be memorized,  
432 being minimized when the minimal distances between the items in the visual stimuli are large. This  
433 prediction will be referred to as the *Prediction of conditional dependence of precision on load*.

434

#### 435 **Testing the prediction of attraction biases**

436 To test the predictions from the model we used the behavioral experiment illustrated in Figure 3A.  
437 The experimental paradigm was adapted from a previously reported paradigm (Bays and Husain  
438 2008) used to investigate the loss of precision with load in a vsWM task in humans. For each trial  
439 the subjects were required to keep in mind the locations of 3 or 4 colored dots positioned on an  
440 invisible circle (stimulus). After presentation of a visual mask, and in some trials after an additional  
441 short delay period (1-3 s), one colored dot reappeared on the invisible circle (probe) and the task  
442 was to judge whether it had been displaced clockwise or counter-clockwise. The average accuracy  
443 on this task was of 70% correct. All subjects performed significantly above chance level, with  
444 accuracies ranging from 59% to 79%.

445 We conducted two tests of the *Prediction of attraction biases*. For the first test we used the trial  
446 types depicted in Figure 3B and labeled them as far (encircled in black) and outwards trials  
447 (encircled in green). In the far trials all items were located far apart from each other. In the outwards  
448 trials the probed item was presented within a visual angle of 4.2 deg from another item, and it was  
449 displaced outwards (or away) from the nearby item (see *Materials and Methods*). In such trials, if  
450 the predicted attraction between bumps of activity corresponding to neighboring items occurred  
451 (Figures 1B, 2A), we expected the memory of any one of these two adjacent items to be biased  
452 towards the middle point between them. As a result, a probe displaced outwards from the  
453 corresponding target, whose memorized location has been attracted to the neighboring item, would  
454 appear to have been subject to a larger displacement than the actual one. This would help the  
455 subject to judge correctly the displacement as *outwards* as opposed to *inwards*. This is

456 schematically depicted in Figure 3D. The bell-shaped curves in Figure 3D represent the probability  
457 distributions of the locations stored in memory over multiple trials of two fixed cue stimulus  
458 configurations, corresponding to far and outwards trial categories, respectively. One can see that the  
459 distance between the mean location of the remembered item and the location of the probe is smaller  
460 for far trials (distance 1) than for outwards trials (distance 2). The location of the probed item  
461 defines an area under the tail of the probability function which is larger for the far trials (area 1)  
462 than for the outwards trials (area 2), and this determines the probability of incorrectly judging the  
463 direction of displacement of the probe. This should result in better performance for outwards trials  
464 than in a control condition without interference, like in far trials. This is indeed what we observed in  
465 our behavioral data set: the fraction of behavioral errors for far trials was significantly larger than  
466 that for outwards trials ( $p = 0.01$ ) (Figure 3C). However, the effect observed could have occurred  
467 before the delay period, during encoding of the visual stimulus. We rejected this explanation by  
468 testing for a difference between trials with and without intervening delay between visual stimulation  
469 and response. We found a significant interaction between trial type (far or outwards) and delay  
470 ( $p = 0.03$ ) and no significant difference between trial types for no-delay trials (Figure 3C).

471 For the second test of the Prediction of attraction biases we used the trial types depicted in  
472 Figure 3E, and labeled them as counter-clockwise (encircled in red) and clockwise (encircled in  
473 blue) trials. In both trial types the probed item was located adjacent to another item. For counter-  
474 clockwise item trials the probed item was located counter-clockwise to the neighboring item, and  
475 for clockwise item trials the opposite was verified. If attraction occurred, we expected the memory  
476 to be biased and the psychometric curves of the two trial types should be horizontally displaced  
477 instead of centered at zero probe displacement. The predicted displacement would be clockwise  
478 (counter-clockwise) for counter-clockwise (clockwise) item trials, indicating that nearby items were  
479 perceived attracted to each other. The data confirmed this prediction (Figure 3F). The two  
480 psychometric curves were significantly different from each other ( $p < 0.0001$ ) and the effect  
481 appeared with delay, as verified by a significant interaction ( $p < 0.0001$ ) between trial type and

482 delay. Note that the magnitude of the attractive bias was indicative of a partial attraction, not a  
483 complete merge of the memories (mean distance between close by items was  $3.2 \pm 0.14$  deg of  
484 visual angle, so a complete merge would correspond to a horizontal displacement by  $1.6 \pm 0.14$  deg  
485 of visual angle in Fig. 2E).

486

#### 487 **Testing the prediction of conditional dependence of precision on load**

488 To test this prediction we used two different trial types having in common that the probed item was  
489 not in close vicinity to any other item (more than 50 deg along the circle). These different trial types  
490 result from the following considerations on the experimental design (for details see *Materials and*  
491 *Methods*). We designed the experiment such that each load condition included a balanced number of  
492 trials with probed item far from or close to neighboring items. The former trials (probed item far)  
493 contained a balanced number of trials with non-probed items in a far or close configuration, giving  
494 rise to the two trial types used in this section. Further, a relatively large part of the circle was  
495 covered by the items in each trial by experimental design, in order to minimize possible effects of  
496 focusing the attention on a restricted arc. Given these constraints, the two trial types had different  
497 inter-item distance properties in relation to load, which we took advantage of to test our second  
498 model prediction. In one trial type (far non-probed items) the minimal distance from the probed  
499 item to other simultaneously presented items was relatively invariant with load (Figure 4A) and  
500 therefore these trials are referred to as balanced trials. In the other trial type (close non-probed  
501 items) the minimal distance between the probed item and other items varied markedly between  
502 loads (Figure 4B) and therefore they are referred to as unbalanced trials. Note that the labels  
503 balanced and unbalanced refer to the distance between probed item and the nearest item being  
504 practically invariant (balanced) or varying significantly (unbalanced) across loads. This difference  
505 is summarized in Figure 4C showing the mean of the minimal distances for the two loads, which is  
506 the same for balanced trials but differs for unbalanced trials. With this set of trials that dissociate  
507 load changes from changes in inter-item distances, we went on to test behavioral performance in the

508 task to validate the model's prediction. We found that there was a significant interaction of trial type  
509 (balanced/unbalanced) and probe displacement on the fraction of correct responses ( $p = 0.05$ ).  
510 Further, we found no difference between the psychometric curves for load 3 and 4 for balanced  
511 trials (Figure 4D) but a difference emerged ( $p = 0.03$ ) for unbalanced trials (Figure 4E). The  
512 difference between the psychometric curves for loads 3 and 4 in unbalanced trials corresponded to a  
513 loss of precision with load (Figure 4F). Precision is here defined as the inverse of the standard  
514 deviation of the cumulative normal curves fitted to the data (Bays and Husain 2008), and it  
515 quantifies the slope of the psychometric curve at zero probe displacement. This loss of precision  
516 was not observed when the distances were balanced across loads (Figure 4F), thus confirming our  
517 second Prediction. The observed differential loss of precision with load for unbalanced trial types  
518 appeared with delay: We verified that there was a significant interaction between delay,  
519 displacement and trial type ( $p = 0.05$ ) and that for the cases with no delay there was no interaction  
520 between trial type and displacement or load. That is, the differences in psychometric curves  
521 observed in trials with delay were not present with no delay.

522

### 523 **Testing a swap-error model**

524 An alternative explanation for the results in Figure 3C and F is that, in some error trials, the subjects  
525 swapped the colors and locations of the two memorized nearby items (Bays et al. 2009, Pertzov et  
526 al. 2012, Ma et al. 2014). Misremembering the binding between color and location would also result  
527 in a reduced fraction of errors for outwards trials. Intuitively, in trials where the color and locations  
528 memories are swapped, the perceived displacement of the probe would be large (the distance  
529 between items plus the actual displacement) and therefore the response would be correct with  
530 higher probability. Thus, we carried out another experiment to contrast this misbinding hypothesis  
531 with the memory attraction hypothesis supported by our computational model.

532 To check for evidence of swap errors in our experimental context, we collected behavioral data  
533 in a variant of the original paradigm (Figure 5A and *Materials and Methods*). In this task, nine

534 participants had to report the remembered locations by controlling a cursor. We quantified  
535 behavioral performance with the standard deviation of the error-to-target distribution, which was  
536  $3.6 \pm 0.6$  degrees of visual angle across subjects (range: 2 to 7.5 deg). If we excluded trials for  
537 which the error to target exceeded 45 degrees along the circle, the error-to-target standard deviation  
538 was  $2.8 \pm 0.4$  degrees of visual angle (range: 1.5 to 5.8 deg).

539 First, we checked that the results shown in Figure 3 were also verified in the modified experimental  
540 paradigm. Indeed, we found that there was a significant difference between the reported errors for  
541 the counter-clockwise and clockwise trial types (Figure 4B,  $p < 0.0001$ ). Similar as in Figure 3, this  
542 data was consistent with attraction of the two memories. We were able to measure the specific  
543 fraction of a perfect merge verified in the data. We did this by normalizing the mean error in each  
544 trials to the distance between close stimuli. The subjects that showed a significant effect (5 out of 9)  
545 presented  $26\% \pm 8\%$  ( $39\% \pm 6\%$ ) of the attraction expected for a total merge of the memories in  
546 clockwise (counter-clockwise) trials.

547 We then fitted behavioral reports with statistical models that included Gaussian-like distributions  
548 around the target memory items (*Materials and Methods*) using a custom expectation maximization  
549 algorithm based on (Bays et al. 2009). For all tested models, the dispersion parameter  $\sigma$  estimated  
550 from trials with close probed items ( $\sigma = 7.63 \pm 0.88$  deg along the circle,  $n=9$ ) did not differ  
551 significantly from that estimated from trials with far probed items (paired t-test,  $p > 0.05$ ,  $n=9$ ),  
552 suggesting that differences in precision between isolated and clustered memory items (Figure 3C)  
553 were not due to different memory resolutions in these two situations. Instead, we tested the  
554 hypothesis that these differences occurred as a result of memory biases caused by neighboring  
555 memories, and we contrasted 3 different models (*Materials and Methods*): an *attraction model*  
556 where responses to the target stimulus experienced a mean bias towards the neighboring memory; a  
557 *swap model*, in which responses to target stimuli were unbiased, but in some trials responses  
558 clustered around the neighboring non-target item; and an *attraction+swap model*, which combined  
559 the two situations: a fraction of swap responses and a mean bias toward neighboring memories

560 (Figure 5C). Note that for the swap model we only considered swaps between close-by items. We  
561 compared the estimated maximum likelihoods of each model using differences in the Akaike  
562 information criterion (AIC, *Materials and Methods*). We calculated this difference between all the  
563 models and the best model. The best model (the one with the lowest AIC) was the *attraction model*  
564 for all but one participant, for which the *attraction+swap model* had the lowest AIC ( $\Delta$ AIC for the  
565 *swap model* was 11.7, i.e. a relative likelihood  $< 0.0001$ ). We excluded this subject to calculate the  
566 average information loss of the *swap* and *merge+swap* models relative to the *attraction model* for  
567 the other participants. The swap model was the worst of the three statistical models tested (Figure  
568 5D). Adding up AICs for these 8 participants, the relative likelihood of the *swap model* compared to  
569 the *attraction model* was below  $10^{-4}$ . These results lead us to discard an explanation based on swap  
570 errors alone for the memory attraction that we demonstrated in Figure 3.

571

#### 572 **Testing repulsion biases**

573 Our model also predicts repulsion for intermediate distances between close-by items (Figure 1B).  
574 This is a result of the limited divergence of inhibitory connections in the network (medium-range  
575 inhibitory connectivity, see *Materials and Methods*). We could test this prediction in our second  
576 experiment. As shown in Figure 6, the interaction between two nearby memories transitioned from  
577 attraction to repulsion as the inter-item distance grew, matching qualitatively our network  
578 simulations (Figure 1B). We computed the memory bias from the psychometric curve fit for each  
579 subject (*Materials and Methods*) and plotted it against distance between items (Figure 6A). Across  
580 subjects, the attractive memory bias of the psychometric curve decreased significantly (one-tailed  
581 paired *t*-test,  $p = 0.02$ ,  $n = 9$ ) from very close memories (3.-3.5 deg of visual angles, memory bias  
582 95% confidence interval [0 0.7] deg, permutation test  $p = 0.05$ ) to slightly more distant ones (4.2  
583 deg of visual angles), at which point the memory bias became marginally negative (memory bias  
584 95% confidence interval [-1.2 0.1] deg, permutation test  $p = 0.07$ ). In addition, we tested significant  
585 memory biases within subjects (*Materials and Methods*), and we found that the number of subjects  
586 with a significant repulsive (attractive) memory bias increased (decreased) with distance between

587 items (Figure 6B, multinomial regression model  $p = 0.035$ , *Materials and Methods*), indicating a  
588 consistent but individually-specific dominance of repulsion for intermediate distances.



## 589 **Discussion**

590

591 In the current study we investigated the neural circuit mechanisms of vsWM limitations by  
592 formulating predictions from a specific neural circuit hypothesis and by testing them in new  
593 behavioral experiments. Specifically, we confirmed model-predicted attractive and repulsive biases  
594 in the recollection of items located nearby in space, and we found that the model-predicted  
595 reduction in vsWM precision caused by the presence of nearby memorized items could explain the  
596 previously reported decrease of vsWM precision with load (Bays and Husain 2008). Taken together,  
597 our results support the encoding of vsWM in sustained activity of topographically organized neural  
598 circuits.

599

### 600 **Item similarity, interference and WM**

601 With this work we contribute to two partially overlapping debates on the behavioral aspects of  
602 visual WM. One of these debates revolves around the impact of similarity and interference between  
603 items, between items and distractors, and items and landmarks on WM performance. Several studies  
604 have demonstrated such effects in vsWM in the presence of landmarks (Werner and Diedrichsen  
605 2002), WM with distractors (Kerzel 2002, Macoveanu et al. 2007, Van der Stigchel et al. 2007,  
606 Herwig et al. 2010 ), memory of sequential items (Papadimitriou et al. 2015), vsWM with memory  
607 manipulation (Oberauer and Kliegl 2006), WM of colors (Johnson et al. 2009, Lin and Luck 2009,  
608 Elmore et al. 2011, Brady and Alvarez 2011), WM of spatial frequency (Viswanathan et al. 2010,  
609 Huang and Sekuler 2010, Mazyar et al. 2012, van den Berg et al. 2012,), WM of sizes (Brady and  
610 Alvarez 2011) and WM of orientation (Johnson et al. 2009, van den Berg et al. 2012). However,  
611 these studies found discrepant results concerning the impact of item similarity and interference. To  
612 our knowledge we are the first to demonstrate a similarity effect for WM of simultaneously  
613 memorized spatial locations: the attraction effect of neighboring items. We have provided evidence  
614 of a detrimental effect of similarity interference on performance, but we identified one specific

615 condition under which the similarity effect results in vsWM performance enhancement: when the  
616 test is presented away from the nearby memorized item (Figure 3C). This is consistent with an  
617 attraction of the representations of memorized nearby locations. The analogy between the attraction  
618 of memories and the previously reported attraction between a memory and a distractor (Herwig et  
619 al. 2010, Macoveanu et al. 2007) and between a memory and an irrelevant previous memory  
620 (Papadimitriou et al. 2015) suggests that distractors compete for a representation in the same  
621 memory circuits as actual memories, similar to the hypothesis of current neural models of vsWM  
622 (Compte et al. 2000, Macoveanu et al. 2007, Cano-Colino et al. 2013).

623 Conceptually, the very existence of similarity effects has led some authors (Elmore et al. 2011,  
624 van den Berg et al. 2012) to interpret them as support for a resources model of WM (Wilken and Ma  
625 2004, Ma et al. 2014), which in its most basic formulation states that WM can be seen as a resource  
626 shared between the memory representations of the different items. Indeed, similarity effects are not  
627 accommodated naturally in the alternative model, the slots model of WM, which states that one  
628 memorizes each item independently until a maximal number of items is reached (Luck and Vogel,  
629 1997, 2013). As some authors have noted, however, similarity or interference effects would not pose  
630 any problem to the slots model if they primarily occurred in the encoding phase, not the mnemonic  
631 phase of the task (Johnson et al. 2009, Lin and Luck 2009). In our experiments, similarity effects  
632 are not present when there is no delay period and the task is otherwise identical. This suggests that  
633 spatial interference of memorized locations occurs during the maintenance of information in WM  
634 and not during the encoding of information. An alternative explanation for the results in Figure  
635 3C,F is that the participants remembered in some trials the colors of two nearby items swapped  
636 (Bays et al. 2009, Pertzov et al. 2012, Ma et al. 2014). To have an idea about how prevalent this  
637 type of errors was in our experimental setup, we ran an additional experiment. We found clear  
638 evidence that swap errors alone cannot explain the prediction of attraction biases and so we  
639 conclude that attraction of memory traces is a more plausible explanation for our results. Note  
640 however, that the amount of swap errors is probably closely related to the specifics of the task and

641 previous studies that found substantial evidence for swap errors did not use vsWM but tasks based  
642 on WM of color (Bays et al. 2009) or orientation (Pertzov et al. 2012).

643

#### 644 **WM precision with load**

645 A second debate concerns the relation between precision of vsWM and number of items to  
646 memorize (WM load), and its implications for the nature of WM. Some authors found a decrease of  
647 precision with load (Bays and Husain 2008, Bays et al. 2009) supporting the resources model  
648 (Wilken and Ma, 2004) of WM, while others found a saturation of precision with load (Zhang and  
649 Luck 2008) supporting models of the family of the slots model (Luck and Vogel 1997, Zhang and  
650 Luck 2008). Crucially, in these slots models information about further items cannot enter WM after  
651 reaching a maximum number of memorized items. Much ongoing research on WM limitations has  
652 focused on resolving the dichotomy between these two alternatives providing new experimental  
653 evidence and leading to further development of algorithmic models, including hybrid models with  
654 characteristics from the slots and resources models (Alvarez and Cavanagh 2004, Xu and Chun  
655 2006, Bays and Husain 2008, Zhang and Luck 2008, Bays et al. 2009, Anderson et al. 2011,  
656 Buschman et al. 2011, Elmore et al. 2011, van den Berg et al. 2012, Luck and Vogel 2013, Ma et al.  
657 2014). A parallel line of research is focusing on the circuit mechanisms of vsWM in biologically  
658 detailed network models (Compte et al. 2000, Macoveanu et al. 2007, Edin et al. 2009, Wei et al.  
659 2012, Bays 2014) that are typically hard to classify into any of these abstract model categories. We  
660 took one such biologically detailed model and we found that the interference between items causes,  
661 on average, loss of memory precision (see also Wei et al. 2012). As the number of items in a  
662 constrained area increases, the probability of having interference between memories increases and  
663 hence a loss of precision with load is observed. The model thus predicts that the decrease of vsWM  
664 precision with load depends largely on the relative location of the items. Our experimental results  
665 were consistent with a distance-dependent relation between precision and load, showing both a  
666 reduction of precision with load (Figure 4E) and a lack thereof (Figure 4D) on the same behavioral

667 data, depending on a selection of trials based on inter-item distance. This suggests that inter-item  
668 distance could be a factor explaining the conflicting results in the literature (Bays and Husain 2008,  
669 Zhang and Luck 2008). Furthermore, our experiments showed that the relationship between spatial  
670 memory precision and load emerged through the delay. This suggests that explanations based on the  
671 processes of memory encoding and decoding (Bays 2014) need to incorporate also the role of  
672 memory maintenance mechanisms.

673

#### 674 **WM model**

675 The network model was used with the same parameters as in (Edin et al. 2009), without further  
676 tuning. We did not seek a quantitative match between the angles or times used for the behavioral  
677 experiments and model simulations. Such a match can be sought by changing parameters of the  
678 model, for example increasing the size of the network would make the values of angular distances  
679 and times in the model approach those of the experiments, at the cost of slower simulations. Such  
680 procedure would make model testing unpractical, without providing any significant conceptual  
681 advantage. Hence, we searched for qualitative robust predictions to test experimentally. Consistent  
682 with this, Wei and coauthors (Wei et al. 2012) working in parallel in a similar model derived  
683 predictions qualitatively in agreement with ours but based on different activity patterns. Indeed,  
684 their model differs from ours fundamentally in that it features a normalization regime where the  
685 same number of active neurons is split among the number of items encoded, with the overall  
686 population activity invariant with load (see also Bays 2014). This is not the regime of operation of  
687 our network, which shows graded rate responses and mean firing rates increasing with load (Edin et  
688 al. 2009). Another difference between the models is that our model, but not the model of Wei et al.  
689 (2012), predicts repulsion between memory traces. Our experimental results (Figure 6) show  
690 evidence for repulsion, hence supporting our model. Further exploration of the regimes where the  
691 two models operate should provide new discriminating predictions to test against experimental data  
692 in the future. Johnson and coauthors (Johnson et al. 2009) also proposed a firing rate model

693 explaining color similarity effects based on a specific decoder mechanism, in contrast with our  
694 model which allocates the mechanism in the dynamics of the circuit during the maintenance phase.  
695 Our experimental results for vsWM show that the similarity effects appear with delay and therefore  
696 are not originated during the encoding or decoding phases of the task. This is consistent with  
697 interference during the active maintenance of memory. We note however that different mechanisms  
698 might be behind the effects described for color (Johnson et al. 2009) or orientation (Bays 2014)  
699 WM tasks. Finally, our model did not simulate all components of the tasks: Our tasks demanded the  
700 binding of two different features (color and position), while the model was only simulating the  
701 storage of position. This is partly because of the lack of a consensual model for feature binding in  
702 working memory, but also because the behavioral effects that we are reporting proved not to depend  
703 crucially on such binding. Indeed, we demonstrate in our last experiment that the attraction effect is  
704 independent of swap errors. This result justifies interpreting our data with a simplified model  
705 representing only location information. However, a complete understanding of this task will require  
706 explicitly simulating the binding component.

707 Our results advance our understanding of vsWM in terms of its neuronal circuit underpinnings by  
708 providing evidence for a critical assumption of an explicit computational model of vsWM. Namely,  
709 that vsWM is supported by a network of neurons organized according to a continuous topography in  
710 terms of internal connectivity and external inputs received. This topographical connectivity enables  
711 the model to sustain a continuous attractor mechanism, on which memories of neighboring items  
712 interfere (Amari 1977). Recently, direct experimental evidence from neural activity in the prefrontal  
713 cortex of monkeys performing a single-item spatial working memory task has been obtained in  
714 favor of this continuous attractor mechanism (Wimmer et al. 2014). Here, the consistency of our  
715 experimental results with the model predictions in the case of multi-item working memory lends  
716 further support to the continuous attractor as the basis of vsWM. Further, the model explains  
717 parsimoniously behavioral effects that cannot be consistently integrated within the prevalent  
718 algorithmic models for vsWM. This underscores the potential of using a circuit-based framework to

719 interpret experimental results on the mechanisms of vsWM.

720

721

## 722 **Funding**

723

724 This work was supported by the Ministry of Economy and Competitiveness of Spain, the European  
725 Regional Development Fund (Ref: BFU2009-09537, BFU2012-34838) and the Karolinska Institutet  
726 Strategic Neuroscience Program. R.A. was supported by the Generalitat de Catalunya (Beatriu de  
727 Pinós program, 2007BP-B100135). The work was carried out at the Esther Koplowitz Centre,  
728 Barcelona.

729

730

## 731 **Acknowledgments**

732

733 We thank Fredrik Edin, Torkel Klingberg, Fiona McNab and Chantal Roggeman for code,  
734 data used in exploratory pilot analyses and valuable discussions of this work.

735

736

737 **References**

- 738 **Akaike H.** A new look at the statistical model identification. *IEEE Transactions on Automatic*  
739 *Control.* 19:716–723, 1974
- 740 **Alvarez G, Cavanagh P.** The capacity of visual short-term memory is set both by visual  
741 information load and by number of objects. *Psychol Sci.* 15:106-111, 2004
- 742 **Amari SI.** Dynamics of pattern formation in lateral-inhibition type neural fields. *Biol Cybernetics.*  
743 *27:77–87, 1977*
- 744 **Anderson D, Vogel E, Awh E.** Precision in visual working memory reaches a stable plateau when  
745 individual item limits are exceeded. *J Neurosci.* 31:1128–1138, 2011
- 746 **Baddeley A.** Working memory. New York: Oxford University Press, 1986
- 747 **Bays P.** Noise in neural populations accounts for errors in working memory. *J Neurosci.* 34: 3632-  
748 3645, 2014
- 749 **Bays P, Catalao R, Husain M.** The precision of visual working memory is set by allocation of a  
750 shared resource. *J Vis.* 9:1–11, 2009
- 751 **Bays P, Husain M.** Dynamic shifts of limited working memory resources in human vision. *Science.*  
752 *321:851–854, 2008*
- 753 **Brady T, Alvarez G.** Hierarchical Encoding in Visual Working Memory: Ensemble Statistics Bias  
754 Memory for Individual Items. *Psychol Sci.* 22:384-92, 2011
- 755 **Burnham K, Anderson D.** Multimodel inference understanding AIC and BIC in model selection.  
756 *Sociological methods & research.* 33:261–304, 2004
- 757 **Buschman T, Siegel M, Roy J, Miller E.** Neural substrates of cognitive capacity limitations. *Proc*  
758 *Natl Acad Sci USA.* 108:11252–11255, 2011
- 759 **Cano-Colino M, Almeida R, Compte A.** Serotonergic modulation of spatial working memory:  
760 predictions from a computational network model. *Front Integr Neurosci.* 7:71, 2013
- 761 **Compte A, Brunel N, Goldman-Rakic P, Wang X-J.** Synaptic mechanisms and network dynamics  
762 underlying spatial working memory in a cortical network model. *Cereb Cortex.* 10:910-923, 2000

763 **Constantinidis C, Franowicz M, Goldman-Rakic PS.** Coding specificity in cortical microcircuits:  
764 A multiple-electrode analysis of primate prefrontal cortex. *J Neurosci.* 21:3646–3655, 2001

765 **Conway A, Kane M, Engle R.** Working memory capacity and its relation to general intelligence.  
766 *Trends Cogn Sci.* 7:547–552, 2003

767 **Dempster A, Laird N, Rubin D.** Maximum likelihood from incomplete data via the em algorithm.  
768 *Journal of the Royal Statistical Society. Series B (Methodological),* 39:1-38, 1977

769 **Eaton J, Bateman D, Hauberg S.** GNU Octave version 3.0.1 manual: a high-level interactive  
770 language for numerical computations. CreateSpace Independent Publishing Platform, 2009

771 **Edin F, Klingberg T, Johansson P, McNab F, Tegnér J, Compte A.** Mechanism for top-down  
772 control of working memory capacity. *Proc Natl Acad Sci USA.* 106:6802–6807, 2009

773 **Elmore L, Ma W, Magnotti J, Leising K, Passaro A, Katz J, Wright A.** Visual short-term  
774 memory compared in rhesus monkeys and humans. *Curr Biol.* 21:975–979, 2011

775 **Funahashi S, Bruce C, Goldman-Rakic PS.** Mnemonic coding of visual space in the monkey's  
776 dorsolateral prefrontal cortex. *J Neurophysiol.* 61:331–349, 1989

777 **Georgopoulos A, Schwartz A, Kettner R.** Neuronal population coding of movement direction.  
778 *Science.* 233:1416-1419, 1986

779 **Herwig A, Beisert M, Schneider W.** On the spatial interaction of visual working memory and  
780 attention: Evidence for a global effect from memory-guided saccades. *J Vis.* 10:1–10, 2010

781 **Huang J, Sekuler R.** Distortions in recall from visual memory: two classes of attractors at work. *J*  
782 *Vis.* 10:1–27, 2010

783 **Inoue M, Funahashi S.** Prefrontal delay-period activity is affected by visual cues presented outside  
784 the memory field. *Neuroreport.* 13:2097–2101, 2002

785 **Johnson J, Spencer J, Luck S, Schöner G.** A dynamic neural field model of visual working  
786 memory and change detection. *Psychol Sci.* 20:568–577, 2009

787 **Kastner S, DeSimone K, Konen C, Szczepanski SW K, Schneider K.** Topographic maps in  
788 human frontal cortex revealed in memory-guided saccade and spatial working-memory tasks. *J*



789 Neurophysiol. 97:3494–3507, 2007

790 **Kerzel D.** Memory for the position of stationary objects: disentangling foveal bias and memory  
791 averaging. *Vis Res.* 159-167, 2002

792 **Lara AH, Wallis JD.** Executive control processes underlying multi-item working memory. *Nat*  
793 *Neurosci.* 17:876-883, 2014

794 **Lee D, Reis B, Seung H, Tank D.** Nonlinear network models of the oculomotor integrator. In  
795 Bower J, editor. *Computational neuroscience, Trends in Research.* Plenum Press, 1997

796 **Lin P, Luck S.** The influence of similarity on visual working memory representations. *Vis Cogn.*  
797 17:356–372, 2009

798 **Luck S, Vogel E.** The capacity of visual working memory for features and conjunctions. *Nature.*  
799 390:279–281, 1997

800 **Luck S, Vogel E.** Visual working memory capacity: from psychophysics and neurobiology to  
801 individual differences. *Trends Cogn. Sci.* 17:391–400, 2013

802 **Ma W, Husain M, Bays P.** Changing concepts of working memory. *Nat. Neurosci.* 17:347-356,  
803 2014

804 **Macoveanu J, Klingberg T, Tegnér J.** A biophysical model of multiple item working memory: a  
805 computational and neuroimaging study. *Neuroscience.* 141:1611–1618, 2006

806 **Macoveanu J, Klingberg T, Tegnér J.** Neuronal firing rates account for distractor effects on  
807 mnemonic accuracy in a visuo-spatial working memory task. *Biol Cybern.* 96:07–419, 2007

808 **Mazyar H, van den Berg R, Ma W.** Does precision decrease with set size? *J Vis.* 12:1–16, 2012

809 **Oberauer K, Kliegl R.** A formal model of capacity limits in working memory. *J Mem Lang.*  
810 55:602–626, 2006

811 **Papadimitriou C, Ferdoash A, Snyder LH.** Ghosts in the machine: memory interference from the  
812 previous trial. *J Neurophysiol* 113:567-577, 2015

813 **Pertsov Y, Dong MY, Peich MC, Husain M.** Forgetting what was where: the fragility of object-  
814 location binding. *PLoS ONE.* 7:e48214, 2012

815 **R Development Core Team.** R: A Language and Environment for Statistical Computing R  
816 Foundation for Statistical Computing, 2013

817 **Schluppeck D, Curtin C, Glimcher P, Heeger D.** Sustained activity in topographic areas of human  
818 posterior parietal cortex during memory-guide saccades. *J Neurosci.* 26:5098-5108, 2006

819 **Tuckwell H.** Introduction to theoretical neurobiology. Cambridge University Press, 1988

820 **Van den Berg R, Shin H, Chou W, George R, Ma W.** Variability in encoding precision accounts  
821 for visual short-term memory limitations. *Proc Natl Acad Sci USA.* 109:8780–8785, 2012

822 **Van der Stigchel S, Merten H, Meeter M, Theeuwes J.** The effects of a task-irrelevant visual  
823 event on spatial working memory. *Psychonomic Bulletin Rev.* 14:1066–1071, 2007

824 **Venables, W, Ripley B.** Modern Applied Statistics with S. 4<sup>th</sup> ed. New York: Springer, 2002

825 **Viswanathan S, Perl D, Visscher K, Kahana M, Sekuler R.** Homogeneity computation: how  
826 interitem similarity in visual short-term memory alters recognition. *Psychon Bull Rev.* 17:59–65,  
827 2010

828 **Warden M, Miller E.** The representation of multiple objects in prefrontal neuronal delay activity.  
829 *Cereb Cortex.* 17:41–50, 2007

830 **Wei Z, Wang X-J, Wang D.** From distributed resources to limited slots in multiple-item working  
831 memory: a spiking network model with normalization. *J Neurosci.* 32:11228–11240, 2012

832 **Werner S, Diedrichsen J.** The time course of spatial memory distortions. *Memory & cognition.*  
833 30:718-730, 2002

834 **Wilken P, Ma W.** A detection theory account of change detection. *J Vis.* 4:1120–1135, 2004

835 **Wimmer K, Nykamp DQ, Constantinidis C, Compte A.** Bump attractor dynamics in prefrontal  
836 cortex explains behavioral precision in spatial working memory. *Nat Neurosci.* 17:431-439, 2014

837 **Xu Y, Chun M.** Dissociable neural mechanisms supporting visual short-term memory for objects.  
838 *Nature.* 440:91–95, 2006

839 **Zemel R, Dayan P, Pouget A.** Probabilistic interpretation of population codes. *Neural*  
840 *Computation.* 10:403–430, 1998

841 **Zhang W, Luck S.** Discrete fixed-resolution representations in visual working memory. *Nature*.  
842 453:233–235, 2008

843 **Figure legends**

844 **Figure 1:** The biophysical network model. (A) Schematic representation of the ring structure of the  
845 network model (left) and of the connectivity structure (right) between excitatory (triangles) and  
846 inhibitory neurons (grey circles). Neurons encoding similar angles were strongly connected as  
847 illustrated by the width of the lines connecting cells. Connections onto excitatory neurons are  
848 indicated with a solid line and onto interneurons with a dashed line, excitatory connections are  
849 indicated in black and inhibitory in grey. (B) Example activity of excitatory neurons in the network,  
850 when items were located in the vicinity of each other leading to attraction of the memory traces.  
851 (C) Example activity of excitatory neurons in the network in a trial with 3 presented items,  
852 illustrating the loss of a memory trace during the delay period.

853

854 **Figure 2:** The biophysical network model predicts behavioral effects in multi-item vsWM tasks.  
855 (A) Memory bias as a function of angle between two items simultaneously presented. The results  
856 are averages over 100 simulations and are based on memory traces after 500 ms from stimulus  
857 offset. Memory biases towards the other presented item (attraction) were defined as positive, while  
858 biases away from the other presented item (repulsion) were defined as negative. The bias for small  
859 angles is easier to explore experimentally and leads to the formulation of the Prediction of attraction  
860 biases. (B) Standard deviation error of the memory trace after 500 ms as a function of load. The  
861 standard deviation error was relatively constant for far items (circles, dashed line) and increased  
862 with load for randomly located items (triangles, solid line), leading to the Prediction of conditional  
863 dependence of precision on load. (C) Proportion of probes judged to be displaced counter-clockwise  
864 from the memorized item. The results are for far items and loads 3 (black) and 4 (gray) and were  
865 fitted with a probit model with displacement of the probe as independent variable. (D) Same as (C)  
866 but for randomly located items. Panels (C) and (D) use the same simulations as in (B) and show that  
867 for far items there is no decrease in precision with load, which is observed for randomly located  
868 items. This observation also leads to the Prediction of conditional dependence of precision on load.

869

870 **Figure 3:** Behavioral data supports the model-derived Prediction of attraction biases. (A) Schematic  
871 illustration of the paradigm used in the behavioral experiment. (B) Illustration of the sorting of trials  
872 according to relative positions of the items. In one case, items were far from each other (far trials,  
873 framed in black). In the other case, the target item was presented close to another item and was  
874 displaced away from its neighbor during probing (outwards trials, framed in green). (C) Fraction of  
875 errors averaged over participants ( $n=8$ ) in 48 trials of each trial type (delay/no delay and  
876 far/outwards). Data was analyzed using a probit model. Significant differences are indicated with a  
877 \*. There was a significant interaction between delay and trial type. For no delay trials there was no  
878 difference between the fraction of errors for far and outward trials, while there was a significant  
879 difference for delay trials. Error bars indicate standard errors of the mean. (D) Schematic illustration  
880 of the mechanism thought to underlie the decrease in errors for outward trials compared with far  
881 trials. The bell-shaped curves represent the probability distribution of the remembered locations.  
882 The probed item defines an area under the probability function. This area is the probability of  
883 incorrectly judging the direction of displacement of the probe and is larger for far than outward  
884 trials ( $a_2 < a_1$ ). The distance between location of the item and location of the probe is larger for  
885 outward trials ( $d_1 < d_2$ ). Hence, the probability of a correct response in outwards trials is larger than  
886 in far trials, as observed experimentally. (E) Illustration of another sorting of trials, all containing  
887 the probed item in the vicinity of another item. Trials were sorted according to the clockwise (blue)  
888 or counter-clockwise (red) location of the probed item relative to the neighboring item. (F)  
889 Psychometric curves for clockwise (blue) and counter-clockwise (red) trials were horizontally  
890 displaced in relation to each other. Curves resulted from a probit model fit to data from all  
891 participants ( $n=8$ ). The results of C and F are consistent with the Prediction of attraction biases.

892

893

894 **Figure 4:** Behavioral data supports the model-derived Prediction of conditional dependence of  
895 precision on load. (A and B) Histograms of the distances between the target or probed item to the  
896 nearest non-probed item for loads 3 (contour only bars) and 4 (filled bars) for the case of balanced  
897 or invariant distances across load, A, or for the case of unbalanced or varying distances across load  
898 trials, B (see Results). Each combination of load and trial type (balanced/unbalanced) included 384  
899 trials. (C) Mean distances from the target to the nearest neighbor for loads 3 and 4 and for balanced  
900 (triangles) and unbalanced (circles) distances. Error bars indicate standard deviations. (D)  
901 Psychometric curves for load 3 (black) and 4 (gray) for the case of balanced distances. Curves  
902 resulted from a probit model fit to data from all participants ( $n=8$ ). (E) The same as in D for  
903 unbalanced distances. (F) Precision derived from panels D, E decreased with load for unbalanced  
904 distances (circles) while it remained unchanged for balanced distances (triangles). Error bars  
905 indicate standard errors of the mean.

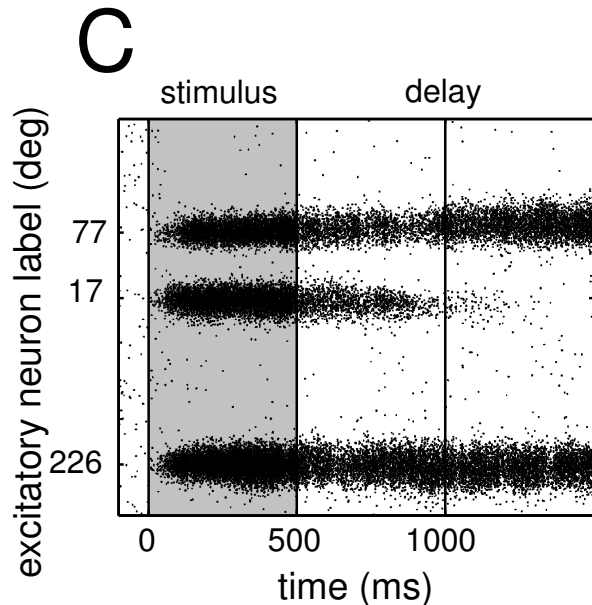
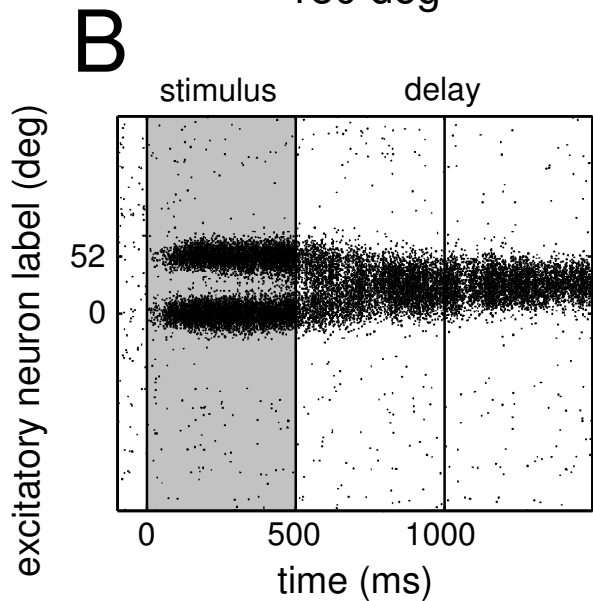
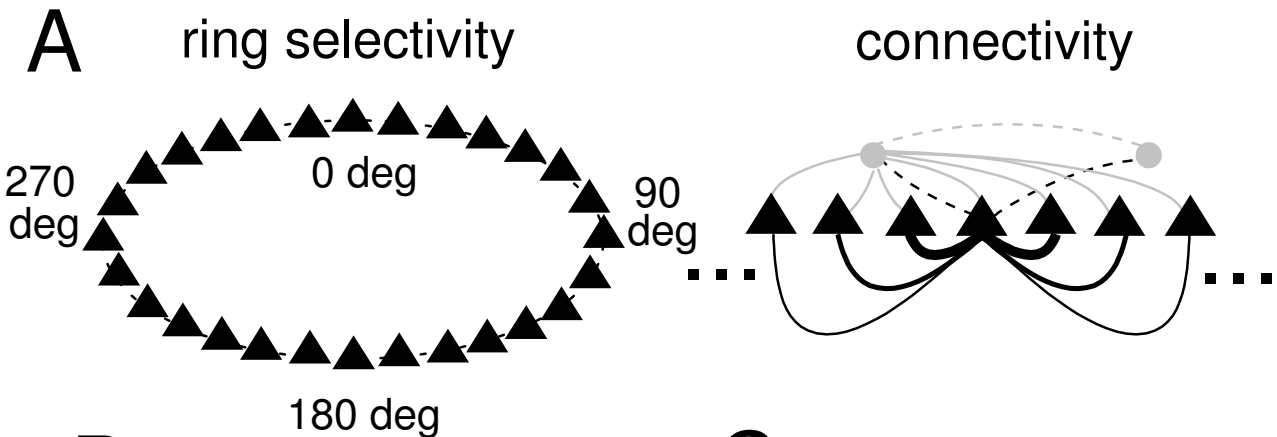
906

907 **Figure 5:** Behavioral data suggests that attraction of memory representations and not swap errors is  
908 responsible for memory biases observed in close trials. (A) Schematic illustration of the modified  
909 experimental paradigm, where participants indicated the remembered target location upon  
910 appearance of a colored cue in the center of the screen. (B) Top: distributions of error to target for  
911 clockwise (gray) and counter-clockwise (black) trials differed significantly ( $p < 0.00005$ , data from  
912 all participants  $n=9$ ), revealing an attractive bias. Bottom: Cumulative proportion of errors to target  
913 from the distributions in top panel, to compare with psychometric curves in Figure 2E. Data was  
914 fitted with a cumulative normal function. (C) Schematic illustration of the probability density  
915 function for each of the 3 models tested. *Swap* (black), attraction (dark gray) and attraction+*swap*  
916 model (light gray). (D) Average information loss  $\Delta AIC$  across subjects ( $n=8$ ) for *swap* and  
917 attraction+*swap* models compared to the attraction model, the best model for data from these  
918 participants.

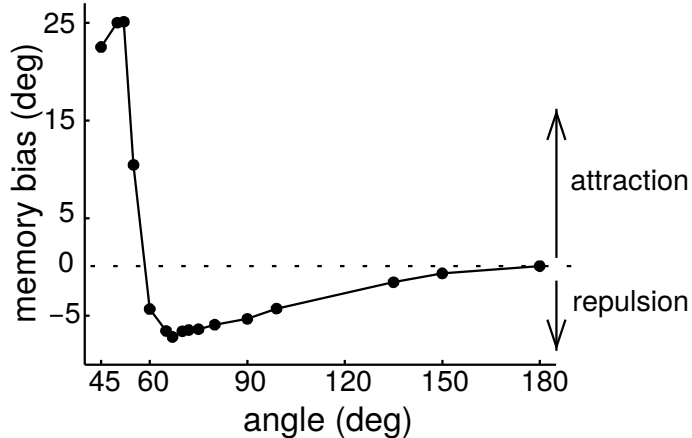
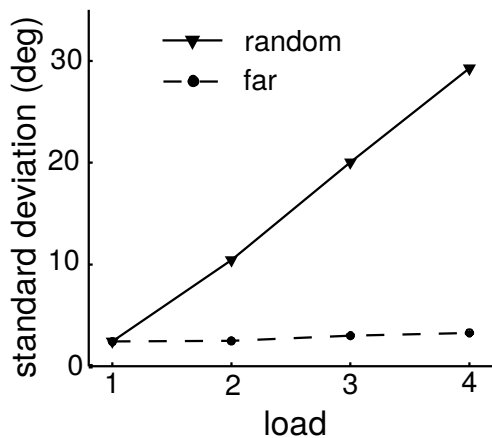
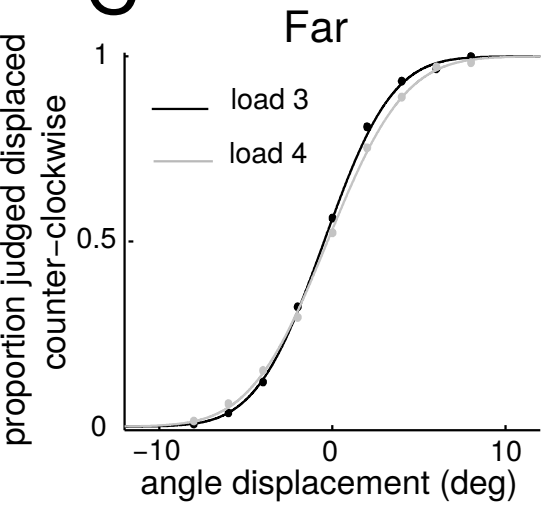
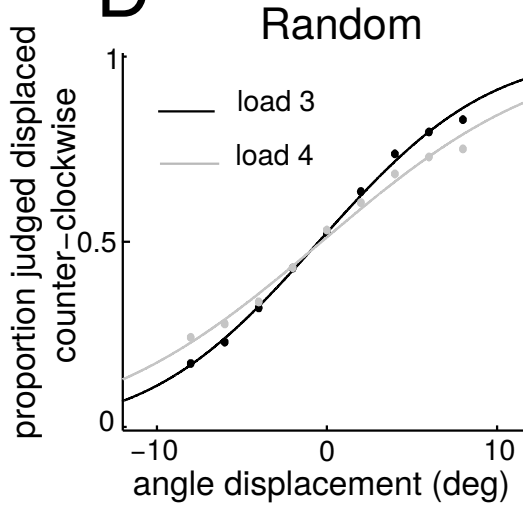
919

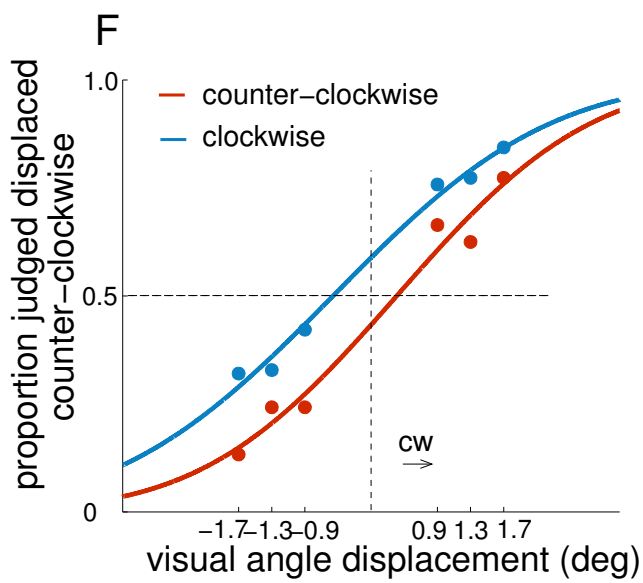
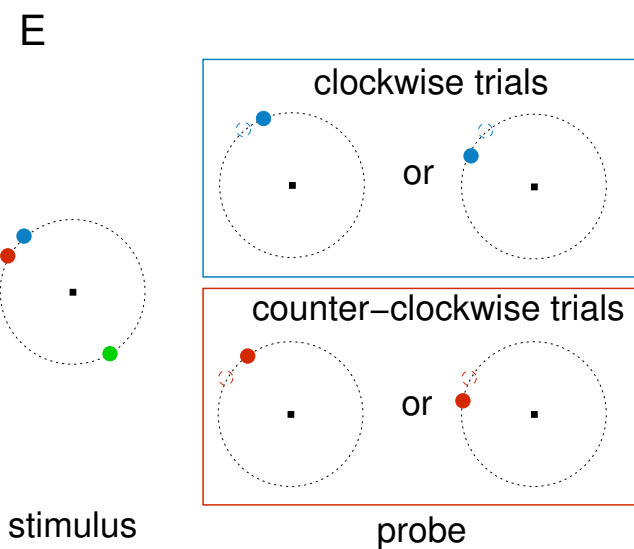
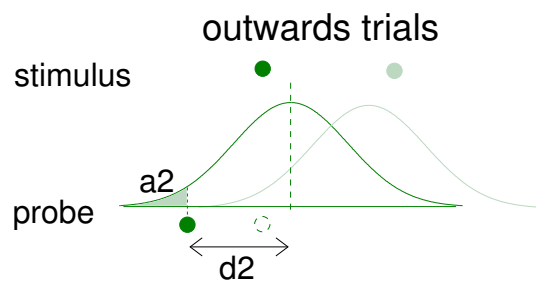
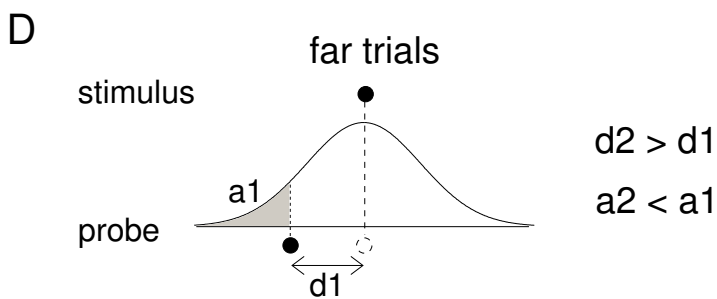
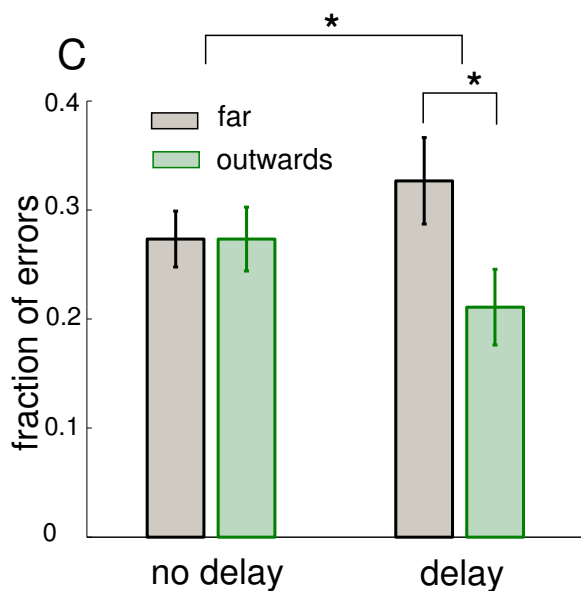
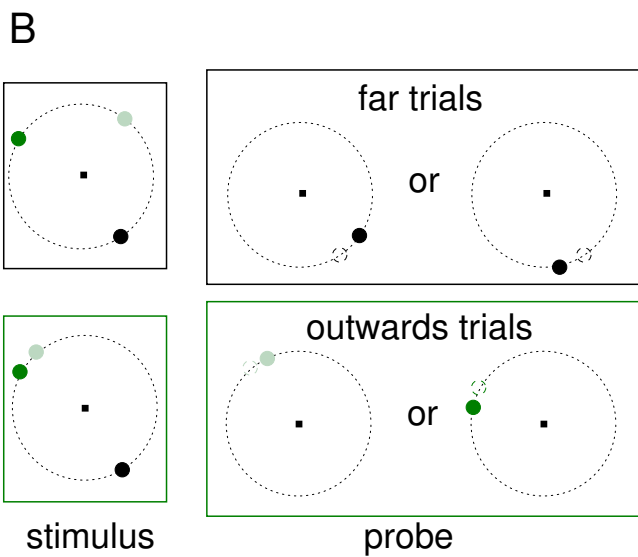
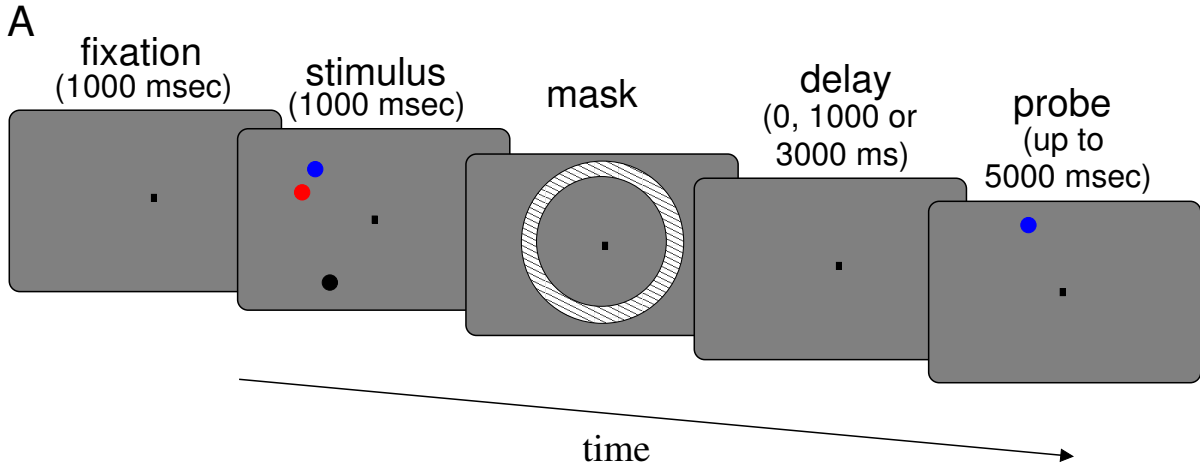
920

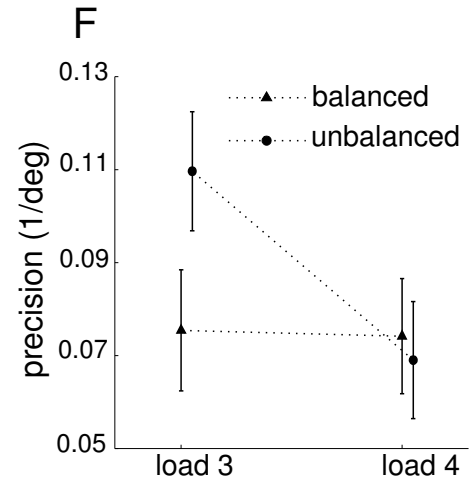
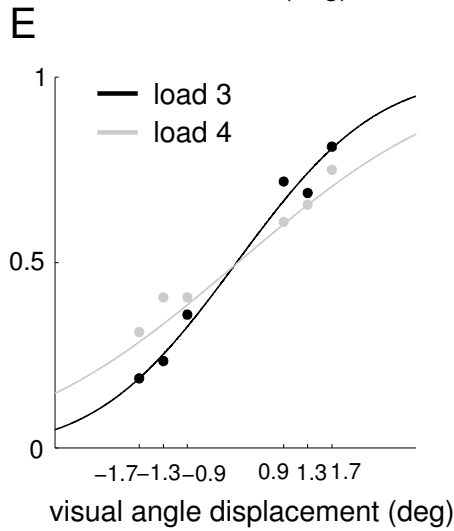
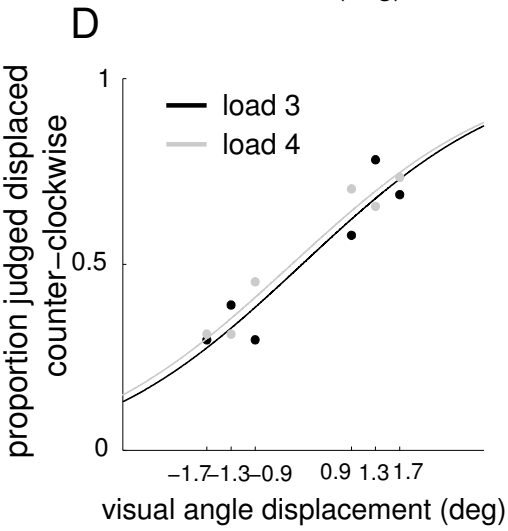
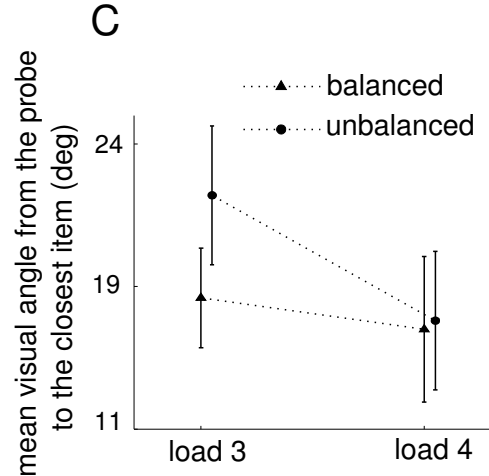
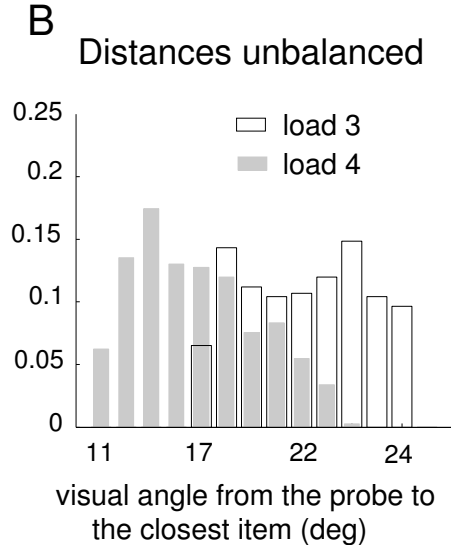
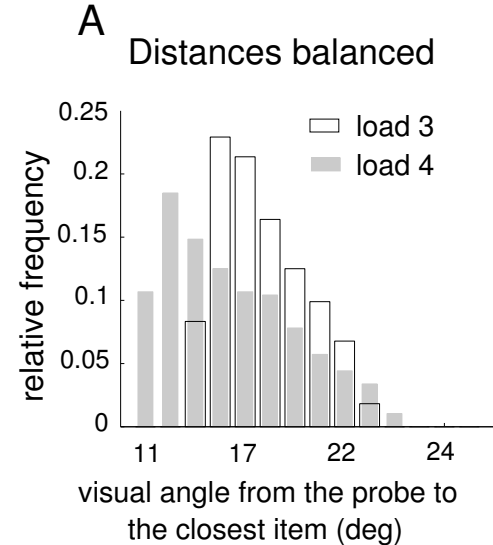
921 **Figure 6:** Memory repulsion emerges for intermediate distances between close-by items. (A)  
922 Subject-averaged memory bias (*Materials and Methods*) for trials with different distances between  
923 memorized close-by items (*x*-axis). Shadows indicate bootstrap-derived 95% confidence intervals.  
924 Stars denote significant difference as evaluated with one-tailed paired *t*-test at  $p < 0.05$ . (B) Number  
925 of subjects with significant (*t*-test  $p < 0.05$ ) attractive and repulsive memory bias in trials with  
926 different inter-item distance.

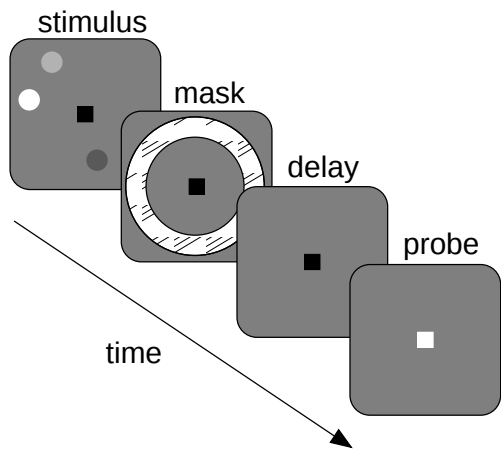
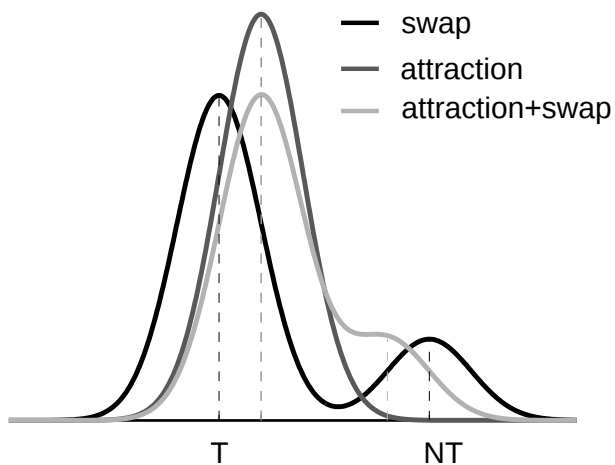
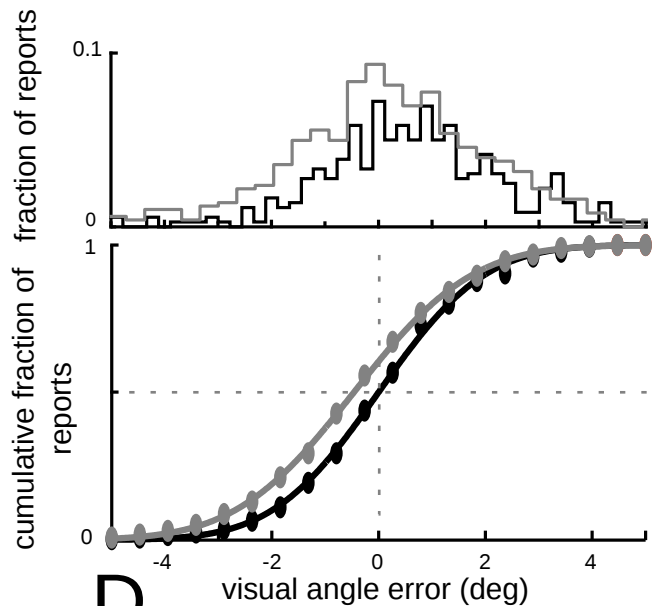




**A****B****C****D**





**A****C****B****D**